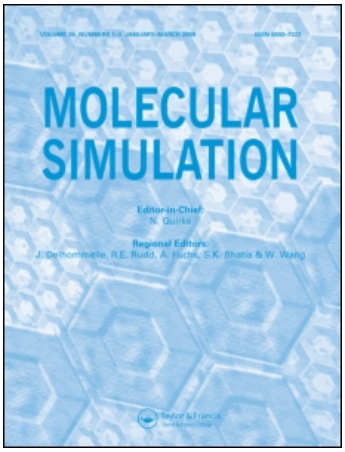

Molecular Simulation

Publication details, including instructions for authors and subscription information:
http://www.informaworld.com/smpp/title~content=t713644482

Compact modeling of symmetrical double-gate MOSFETs including carrier confinement and short-channel effects

D. Munteanu[a]; J. L. Autran[ab]; X. Loussier[a]; S. Harrison[c]; R. Cerutti[c]
[a] L2MP, Marseille Cedex 13, France [b] Institut Universitaire de France (IUF), Paris, France [c] STMicroelectronics, Crolles, France

To cite this Article Munteanu, D. , Autran, J. L. , Loussier, X. , Harrison, S. and Cerutti, R.(2007) 'Compact modeling of symmetrical double-gate MOSFETs including carrier confinement and short-channel effects', Molecular Simulation, 33: 7, 605 — 611
To link to this Article: DOI: 10.1080/08927020600930524
URL: http://dx.doi.org/10.1080/08927020600930524

Molecular Simulation, Vol. 33, No. 7, June 2007, 605–611

Taylor & Francis
Taylor & Francis Group

Compact modeling of symmetrical double-gate MOSFETs including carrier confinement and short-channel effects

D. MUNTEANU†*, J. L. AUTRAN†‡, X. LOUSSIER†, S. HARRISON†¶ and R. CERUTTI¶

†L2MP, 49 rue Joliot-Curie, BP 146, 13384 Marseille Cedex 13, France
‡Institut Universitaire de France (IUF), Paris, France
¶STMicroelectronics, 850 rue J. Monnet, 38926 Crolles, France

(Received June 2006; in final form July 2006)

A compact model for the drain current and node charges in symmetrical Double-Gate (DG) MOSFET, including short-channel and carrier confinement effects is developed. The model is particularly well adapted to ultra-scaled devices, with short-channel lengths and ultra-thin silicon films. An extensive comparison step with 2D quantum numerical simulation fully validates the model. The model is also shown to reproduce with an excellent accuracy experimental drain current measured in DG devices fabricated with Silicon-on-Nothing (SON) process. Finally, the DG model has been successfully implemented in Eldo IC analog simulator, demonstrating the application of the model to circuit simulation.

Keywords: Compact modeling; Double-Gate MOSFET; Quantum effects; Short-channel effects

1. Introduction

Double-Gate (DG) structure has been in the last years the object of intensive research and an impressing number of studies have confirmed its enormous potentiality to push back the integration limits to which conventional devices are subjected [1–4]. The main advantage of this architecture is to offer a reinforced electrostatic coupling between the conduction channel and the gate electrode. In other terms, a DG structure can efficiently sandwich (and thus very well control, electrostatically-speaking) the semiconductor element playing the role of the transistor channel, which can be a silicon thin layer or nanowire, a carbon nanotube, a molecule or an atomic linear chain. The MOSFET operation of such ultimate DG devices with a single quantum conduction channel has been theoretically demonstrated in recent works [5,6].

Although the operation of DG transistor is similar to the conventional MOSFET, the physics of DG MOSFET is more complicated. Moreover, physical phenomena such as 2D electrostatics or carrier quantization have to be considered, since DG structure will be precisely used to design very integrated devices (with short-channel and extremely thin films). Therefore, new compact models, dedicated to the circuit simulation, have to be developed for DG MOSFET [4]. Several interesting models have been proposed for the classical (i.e. without quantum effects) drain current in long channels DG [3,4,7–9] or for short-channel DG operating in the subthreshold regime [10]. Carrier quantization effects have been considered for the first time in Ref. [11]. In this work, we propose a compact model, which combines short-channel with quantum-mechanical effects and applies to all operation regimes. In addition the model is continuous over all gate and drain bias range, which makes it very suitable for implementation in circuit simulators. The development is based on the calculation of the 2D potential distribution in the device taking into account the quantum-evaluated inversion charge. A full 2D quantum mechanical numerical simulation code [12] is used for completely validating the model. The drain current as predicted by the model is compared with experimental data measured on scaled DG devices fabricated using the Silicon-on-Nothing (SON) process [13,14]. Finally, the drain current model is supplemented by a node charge model and further, the entire DG model is successfully implemented in Eldo IC analog simulator.

*Corresponding author. Tel.: + 33-4-96-13-98-19. Fax: + 33-4-96-13-97-09. Email: munteanu@up.univ-mrs.fr

Molecular Simulation
ISSN 0892-7022 print/ISSN 1029-0435 online © 2007 Taylor & Francis
http://www.tandf.co.uk/journals
DOI: 10.1080/08927020600930524

2. Drain current modeling

The schematic of a symmetric DG structure and its parameters are shown in figure 1(a). Figure 1(b) illustrates the band diagrams in an horizontal cross-section together with the first energy subbands. The drain current modeling starts with the calculation of the 2D potential distribution in the DG transistor. For this purpose several methods have been proposed, the most complete being the evanescent-mode analysis, where the potential is divided into two different parts $\Psi(x,y) = \Psi_L(y) + \Psi^*(x,y)$ [15]. The first term represents the long channel solution and the second term takes into account short-channel behavior. This last term is then approximated by retaining only the lowest-order mode from a Fourier expansion of modes. The method can be very powerful for taking into account short-channel effects in the evaluation of the threshold voltage [15], but the mathematical development is complicated. For simplifying the calculation, in this work we assume the following dependence for the potential:

$$\Psi(x,y) = \Psi_s(x) \times \mathrm{VE}(x,y) \tag{1}$$

where Ψ_S is the surface potential and $\mathrm{VE}(x,y)$ is the vertical distribution envelope function. The 2D potential distribution is thus obtained by modulating the surface potential by an envelope function containing the potential dependence in the vertical direction. $\mathrm{VE}(x,y)$ is then given by:

$$\mathrm{VE}(x,y) = \frac{P(x,y)}{P(x,y=0)} \tag{2}$$

where $P(x,y)$ is calculated as in Ref. [16]:

$$P(x,y) = \psi_0 - \frac{2}{\beta}\ln\left\{\cos\left[\sqrt{\frac{q^2 n_i}{2kT\varepsilon_{Si}}}\mathrm{e}^{(\beta(\psi_0 - \mathrm{QFL}(x))/2)}\left(y - \frac{t_{Si}}{2}\right)\right]\right\} \tag{3}$$

where $\beta = q/kT$, $\mathrm{QFL}(x)$ is the quasi-Fermi level and ψ_0 are calculated as shown in Ref. [16].

For calculating the vertical distribution envelope function $\mathrm{VE}(x, y)$, the expression of $\mathrm{QFL}(x)$ is needed. An analytical expression of $\mathrm{QFL}(x)$ has been proposed in Ref. [17] for bulk MOSFET, depending on the x-position in the channel, on the channel length and on the drain voltage. However, our detailed investigation by numerical simulation showed that the quasi-Fermi level in DG MOSFET also depends on the gate voltage and on the film thickness. Therefore, we adopted here a quasi-empirical expression (equation (4)) inspired from that proposed in Ref. [17] and extensively verified by numerical simulation:

$$\mathrm{QFL}(x) = \frac{2kT}{q} m \ln\left[\left(\exp\left(-\frac{V_D/m}{kT/q}\right) - 1\right)\left(\frac{x}{L}\right)^{(c/V_G - V_{FB})} + 1\right]^{-1} \times (at_{Si})^{(V_D/3c)} \tag{4}$$

where $m = 2 + b(V_G - V_{FB})$, $a = 0.2\,\mathrm{nm}^{-1}$, $b = 7.5\,\mathrm{V}^{-1}$ and $c = 1\,\mathrm{V}$.

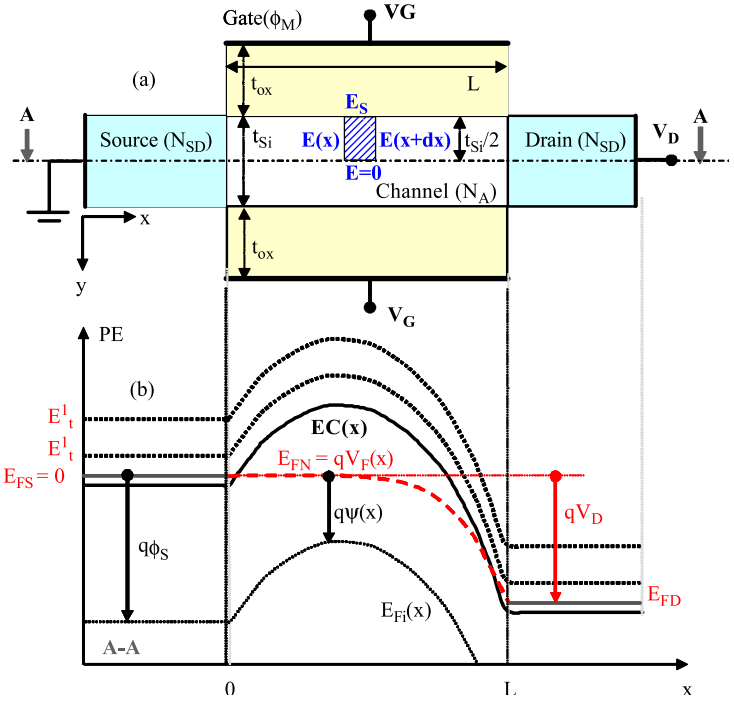

Figure 1. (a) Schematic of symmetrical DG MOSFET structure and its electrical and geometrical parameters considered in this work; the dashed area shows the closed surface for the application of the Gauss's law; and (b) band diagram in a vertical cross-section in the channel and definition of the different parameters used in the model development.

The last term to be calculated for obtaining the 2D potential distribution is the surface potential $\Psi_S(x)$. As presented in Ref. [18], for obtaining the expression of $\Psi_S(x)$ the Gauss's law is applied to the particular closed surface shown in figure 1(a):

$$-E(x)\frac{t_{Si}}{2}+E(x+dx)\frac{t_{Si}}{2}-E_S(x)dx = -\frac{qN_A t_{Si}dx}{2\varepsilon_{Si}}-\frac{Q_i(x)dx}{2\varepsilon_{Si}} \quad (5)$$

where $E(x)$ is the electric field, $E_S(x)$ is the surface electric field at the Si/SiO_2 interface and N_A is the channel doping. $Q_i(x)$ is the inversion charge density in the x point of the channel, calculated by the integration of the electron charge over the Si film thickness. In the right hand side of equation (5), the first term corresponds to the depletion charge and the second term corresponds to the mobile inversion charge.

It has been shown in Ref. [13] that for very thin films (<15 nm), the electric field $E(x)$ in equation (5) can be approximated as:

$$E(x)\approx -\frac{d\Psi_s(x)}{dx} \quad (6)$$

The following equation can also be written for the electric field:

$$\frac{-E(x)+E(x+dx)}{dx}=\frac{dE(x)}{dx} \quad (7)$$

In equation (10), the surface electric field at the interface Si/SiO_2, $E_S(x)$, is obtained from the boundary conditions at the interface:

$$V_G - V_{FB} = \frac{\varepsilon_{Si}}{\varepsilon_{ox}}t_{ox}E_s + \Psi_s + \phi_F \quad (8)$$

where V_{FB} is the flat-band voltage and ϕ_F is the Fermi potential. Replacing equation (6) in equation (7) and then in equation (5) and using equation (8), we obtain the following differential equation for the surface potential Ψ_S:

$$\frac{d^2\Psi_s}{dx^2}-\frac{2C_{ox}}{\varepsilon_{Si}t_{Si}}\Psi_s = \frac{1}{\varepsilon_{Si}t_{Si}}[qN_A t_{Si}-2C_{ox}(V_G-V_{FB}-\phi_F)+Q_i] \quad (9)$$

An approximative analytical solution of equation (9) is given by:

$$\Psi_s(x)=C_1\exp(m_1x)+C_2\exp(-m_1x)-\frac{R(x)}{m_1^2} \quad (10)$$

with C_1, C_2, m_1 and $R(x)$ calculated for filling the boundary conditions $\Psi_S(x=0)=\phi_S$ and $\Psi_S(x=L)=\phi_S+V_D$:

$$C_{1,2} = \pm\frac{\phi_S[1-\exp(\mp m_1L)]+V_D+R(0)(1-\exp(\mp m_1L)/m_1^2}{2\sin h(m_1L)} \quad (11)$$

$$R(x)=\frac{qN_A t_{Si}-2C_{ox}(V_G-V_{FB}-\phi_F)+Q_i(x)}{\varepsilon_{Si}t_{Si}} \quad (12)$$

$$m_1=\sqrt{2C_{ox}/(\varepsilon_{Si}t_{Si})} \quad (13)$$

$$\phi_S=(kT/q)\ln\left(N_A N_{SD}/n_i^2\right) \quad (14)$$

The evaluation of $R(x)$ requires to know the value of the inversion charge density $Q_i(x)$, which can be calculated in two different cases: (a) the "classical" case, i.e. without quantum confinement effects; and (b) the quantum case. In the classical case, the inversion charge is given by the following equation, assuming a Boltzmann distribution for the carriers in the channel:

$$Q_i(x)=\int_0^{t_{Si}} qn_i e^{(q/KT)[(\Psi(x,y)-QFL(x))]}dy \quad (15)$$

In the quantum case, the inversion charge $Q_i(x)$ is given by:

$$Q_i(x)=\frac{qkT}{\pi\hbar^2}\sum_{l,t}\sum_i m_{2D}^{t,l}g_{t,l} \times\ln\left[1+\exp\left(-\beta\left(\xi_{l,t}^i+\frac{E_g}{2}-\Psi_S(x)+QFL(x)\right)\right)\right] \quad (16)$$

where $m_t^*=0.19\times m_0$, $m_1^*=0.98\times m_0$, $g_l=2$, $g_t=4$, $\beta=q/kT$, $m_{2D}^l=m_t^*$, $m_{2D}^t=\sqrt{m_l^* m_t^*}$. In equation (16) $\xi_{l,t}^i$ are the energy levels calculated using a standard method for first-order perturbation applied to the energy levels of an infinite rectangular well (as shown in Ref. [13]):

$$\xi_{l,t}^i=(\xi r)_{l,t}^i+\Delta\xi^i \quad (17)$$

where $(\xi r)_{l,t}^i$ are the energy levels of an infinite rectangular well. $(\xi r)_{l,t}^i$ is given by the well-known equation:

$$(\xi r)_{l,t}^i=\frac{\hbar^2\pi^2 i^2}{2qm_{l,t}^* t_{Si}^2} \quad (18)$$

and

$$\Delta\xi^i=\langle\varphi^i|H|\varphi^i\rangle \quad (19)$$

where H is the Hamiltonian of the perturbation and ϕ^i are the electron wave functions associated to energy levels $\xi_{l,t}^i$. In equation (11), $R(0)$ is calculated considering $Q_i(0)$ given by equations (15) or (16) with $\Psi_S(0)=\phi_S$.

Since $\Psi_S(x)$ given by equation (10) depends on $Q_i(x)$, replacing equations (10) and (17) in equation (16) leads to an implicit equation on $Q_i(x)$, which is solved numerically for obtaining $Q_i(x)$. Finally, for calculating the drain current in DG MOSFET we express the current density (including both the drift and the diffusion components) as:

$$J=-q\mu n(x,y)\frac{d\,QFL(x)}{dx} \quad (20)$$

which is then integrated in y- and z-directions:

$$I_d(x)=\mu W Q_i(x)\frac{d\,QFL(x)}{dx} \quad (21)$$

Current continuity requires the drain current be independent of x and therefore, integrating equation (21) in x-direction from $x=0$ to $x=L$ gives the final expression of I_D:

$$I_D=\mu\frac{W}{L}\int_0^{V_D}Q_i(x)d\,QFL(x) \quad (22)$$

In the classical case and considering the Boltzmann distribution for the carriers, equation (21) becomes [10]:

$$I_D = \mu W \frac{kT}{q} \frac{1 - \exp(-qV_D/kT)}{\int_0^L (dy / \int_0^{t_{Si}} q n_i e^{q\psi(x,y)/kT} dx)} \qquad (23)$$

3. Model validation by numerical simulation: short-channel, quantum effects and volume inversion

The model was validated by an extensive comparison with quantum numerical simulation using a full 2D Poisson–Schrödinger code [12]. In a first step, the potential distribution as given by equation (1) has been extensively validated for various structure parameters and biases. An example is shown in figure 2(a), where the surface potential as given by the model for $L = 50$ and $L = 100$ nm is compared with numerical simulation. In figure 2(b), the potential distribution in a vertical cut-line perpendicular to the Si film (in the middle of the channel, y-direction) is illustrated. A good agreement is obtained between the model and the numerical simulation. The variation of the quasi-Fermi level (equation (4)) was also validated as presented in figure 3. Equation (3) has been derived under classical assumptions, but we verified by quantum numerical simulation that this equation still applies in the quantum case.

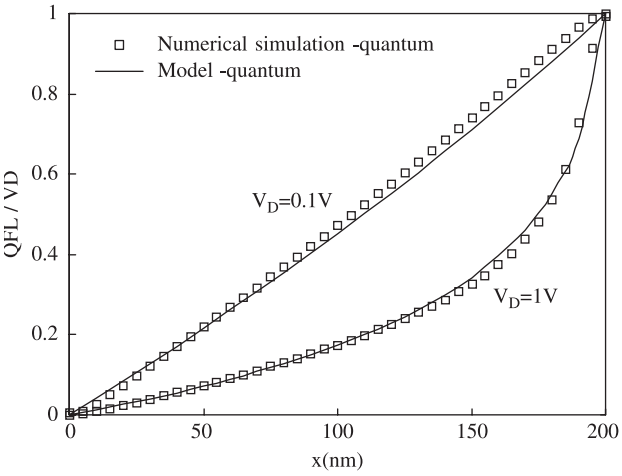

Figure 3. Variation with x of the normalized quasi-Fermi level QFL/V_D for $L = 200$ nm (intrinsic channel) at low and high drain voltage.

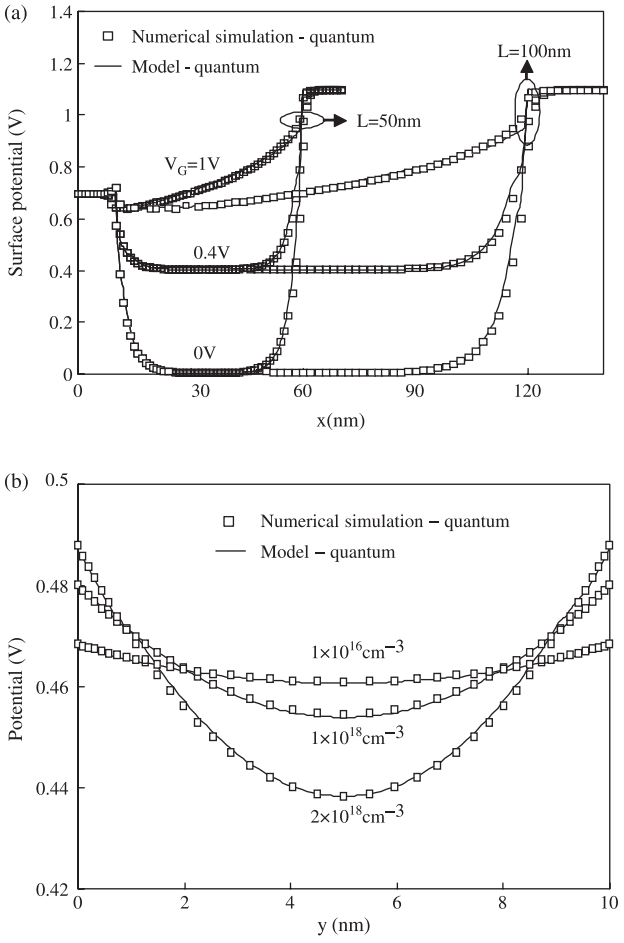

Figure 2. (a) Surface potential variation along the channel from source to drain for $L = 50$ and $L = 100$ nm ($t_{Si} = 5$ nm, $V_D = 0.4$ V). (b) Potential variation the y-direction for different channel doping levels ($t_{Si} = 10$ nm, $V_G = 0.6$ V). Comparison between compact model and numerical simulation.

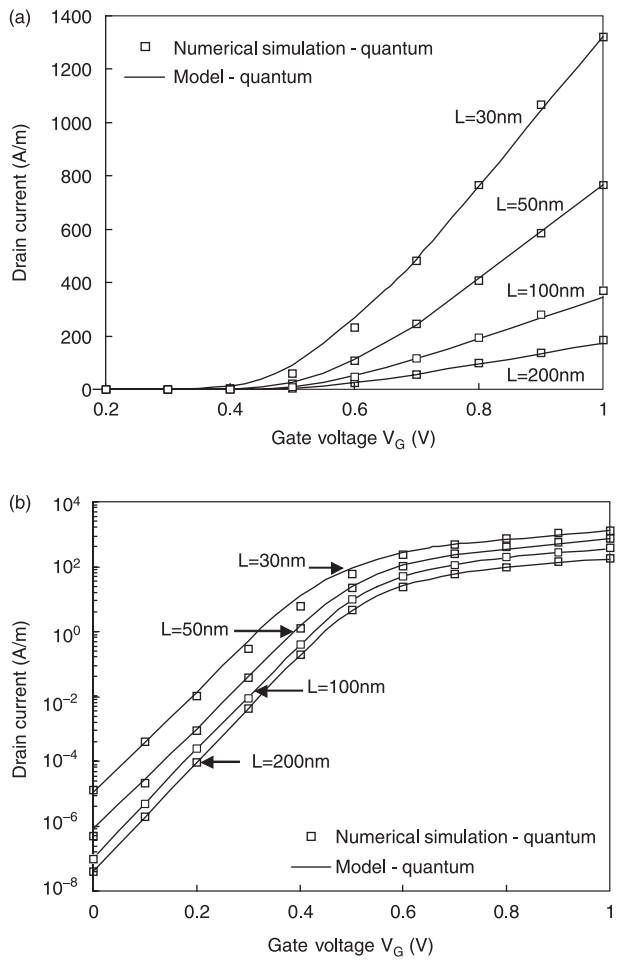

Figure 4. Drain current in long and short channel DG transistors as calculated by model in the quantum case and validation by numerical simulation ($t_{Si} = 10$ nm, $t_{ox} = 1$ nm, midgap gates, intrinsic channel, $V_D = 0.1$ V).

In a second step, the drain current expression has been completely validated by numerical simulation, for channel lengths varying between 30 and 200 nm and film thicknesses from $t_{Si} = 15$ nm down to $t_{Si} = 2$ nm. Figure 4 shows an example of this validation step on DG MOSFET with different channel lengths (a constant mobility is considered in equation (22)). Short-channel behavior of the quantum drain current is also checked in figure 4: the model reproduces very well the simulation (even for $L = 30$ nm), in both weak and strong inversion regimes. The extensive investigation of additional $I_D(V_D)$ curves has shown that the model is completely valid in both linear and saturation regimes.

The validation procedure was continued by an in-depth investigation of the model capability to take into account carrier quantization effects. For this purpose the inversion charge density $Q_i(x)$ (in both classical and quantum case) in long and short-channels has been compared to numerical results and very good agreement has been found (figure 5). Further the classical and quantum drain current were calculated as a function of the channel thickness t_{Si}. Figure 6 shows that the quantum model perfectly reproduces two essential phenomena:

(1) The impact of quantum effects quantum effects, increasingly significant when t_{Si} is scaled down. The shift between classical and quantum $I_D(V_G)$ curves increases for thinner Si channels. In the same way, the shift between the classical and the quantum threshold voltage is clearly higher for $t_{Si} = 2$ nm than that for $t_{Si} = 10$ nm.

(2) The drain current dependence on the channel thickness in the subthreshold region, as a manifestation of the volume inversion, which is a key phenomenon in symmetrical DG transistors. Above threshold the drain current does not depend much on the Si channel thickness [7].

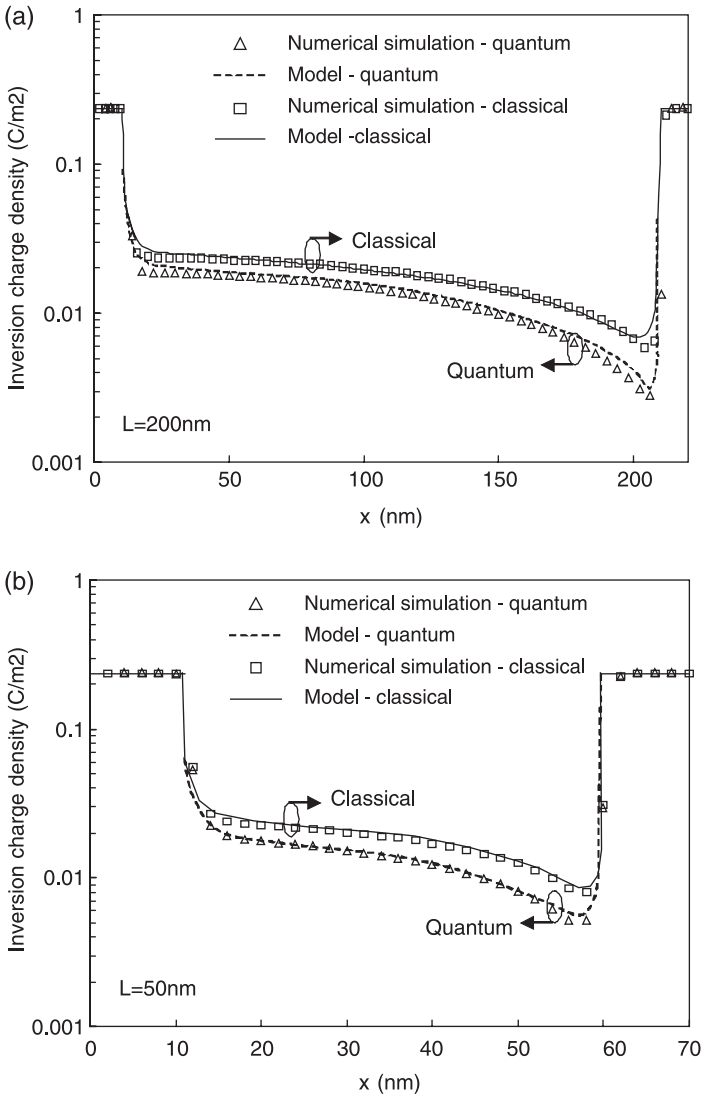

Figure 5. Variation of the inversion charge density $Q_i(x)$ along the channel from source to drain in the classical and quantum mechanical cases: (a) $L = 200$ nm; (b) $L = 50$ nm. Other parameters are: $t_{Si} = 5$ nm, $V_G = 1$ V, $V_D = 0.4$ V, intrinsic channel.

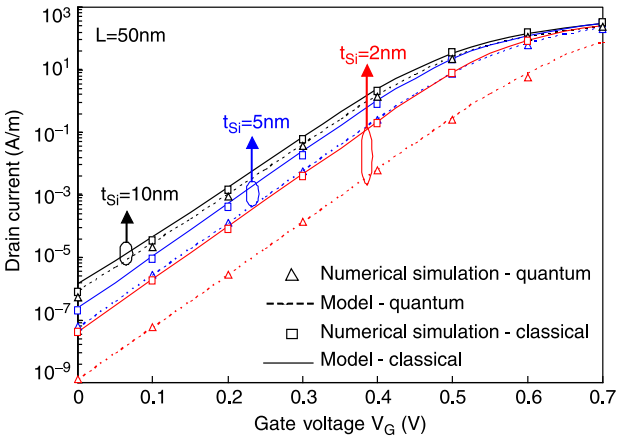

Figure 6. Impact of film thickness on the subthreshold operation of $L = 50$ nm DG transistor: the model perfectly reproduces quantum effects and volume inversion ($t_{ox} = 1$ nm, midgap gates, intrinsic channel). The drain current calculated in the classical case is also shown.

4. Compact model versus experimental data

Finally, the model was used to fit drain current measured [13,14] on DG devices (figure 7). The match between experiment and model is very good, especially in the subthreshold regime. Above threshold the model slightly overestimates the current due to the use of a constant mobility and no series resistances. For improving the model accuracy the next step will be to consider a realistic mobility model [19] and to include the effect of series resistances.

The proposed compact model can easily be used to obtain all main performance indicators of DG MOSFET, such as the threshold voltage V_T, the subthreshold swing S, the drain-induced-barrier-lowering (DIBL) effect on the threshold voltage, the threshold voltage roll-off, I_{on} and I_{off} currents and the CV/I metric. In addition, the model can be directly implemented in circuit simulation software and used for the simulation of DG MOSFET-based circuits, as will be shown in following paragraph.

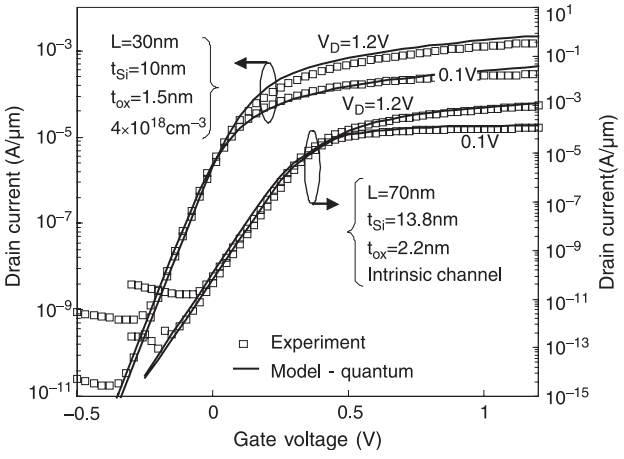

Figure 7. Compact model versus experimental data measured on DG transistors fabricated with the GAA/SON process described in Ref. [13,14].

5. Model implementation in Eldo™ IC analog simulator

The drain current model presented previously has been implemented in a circuit simulator in order to evaluate the performances of simple DG MOSFET-based circuits. For this purpose, the model was firstly supplemented by a charge model including the expressions of charges on the device terminals. The schematic description of the entire model is given in figure 8(a) as well as the symbol of a DG transitor with *n*-channel. In this figure Q_G is the total charge on the two gates, Q_D is the charge on the drain terminal and Q_S is the charge on the source terminal.

The starting point for calculating the gate charge is the neutrality condition which requires that the total charge in

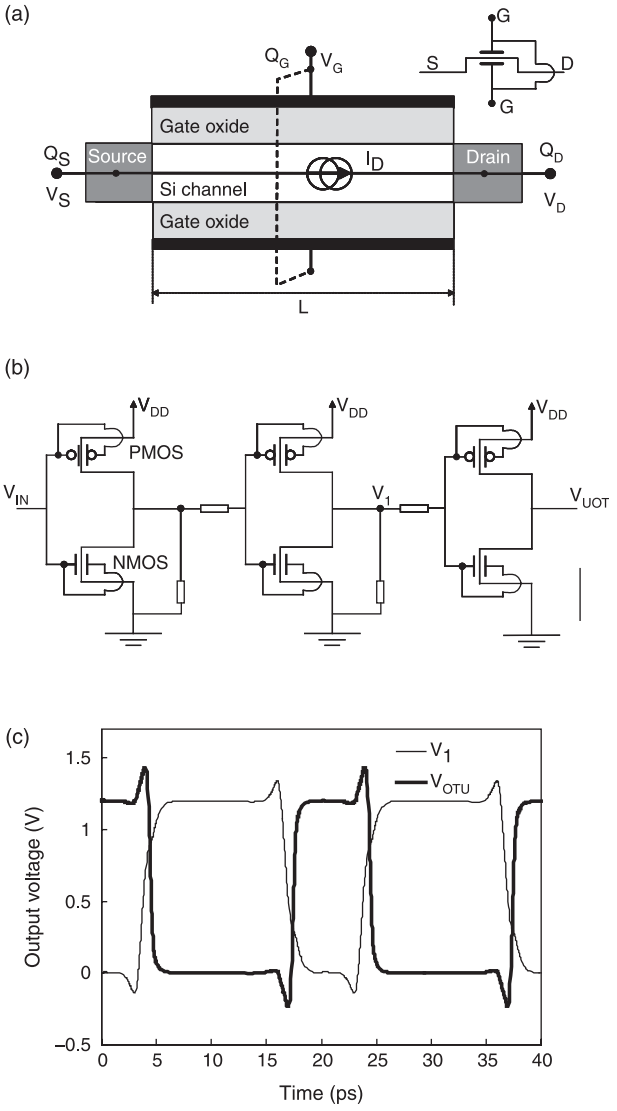

Figure 8. (a) Schematic description of the DG model implemented in Eldo IC analog simulator and definition of the node charges. The symbol of a DG MOSFET with *n*-channel is also represented. (b) Schematic of a three-stage inverter chain containing DG MOSFETs with *n*- and *p*-channels. (c) Transient analysis of the three-stages inverter chain shown in figure (b) and simulated using the model: response to a rectangular input voltage V_{IN}. The parameters of DG transistors are: $L = 50$ nm, $t_{Si} = 10$ nm, $t_{ox} = 1.5$ nm, intrinsic channel and midgap gates.

the device be always zero:

$$Q_G + Q_I = 0 \tag{24}$$

In equation (24) Q_I is the total inversion charge obtained by the integration of relation (16) from 0 to L:

$$Q_I = \int_0^L Q_i(x)\mathrm{d}x \tag{25}$$

The gate charge Q_G is then obtained from equation (24). Under normal bias conditions, the inversion charge is not uniformly distributed along the channel except for $V_D = V_S$. Because of this bias dependence, $Q_i(x)$ contributes differently to the source and drain charges. Various approaches have been proposed for sharing the inversion charge between the source and drain nodes [20–22]. In our development we have adopted the approach given in Ref. [22] and also presented in Ref. [18]. At low drain voltage, the inversion charge is equally shared between the source and drain. When the drain voltage increases, the drain charge is strongly reduced and the source charge becomes close to the inversion charge Q_I.

It is important to note that our compact model is completely continuous over all operation regimes and the drain current and node charges equations are derivable and their derivatives are also continuous over all bias regimes. We have also verified that the source and the drain electrodes can be permuted.

The compact model described previously for the n-channel DG transistor (NMOS) has been implemented in Eldo IC simulator. A similar model has been considered for the DG MOSFET with p-channel (PMOS). The model has been used further to simulate DC and transient response of a three-stage inverter chain containing DG MOSFETs (the schematic of this circuit is shown in figure 8(b)). The figure 8(c) shows the time response of the two outputs voltages (the output voltage of the second and of the third stages) to a rectangular input voltage. This results demonstrates that the model can be perfectly used to the simulation of small circuit based on DG MOSFETs.

6. Conclusion

In this paper, we developed a compact model for the drain current and node charges in symmetrical DG transistors, including short-channel and carrier quantization effects. The model is particularly dedicated to ultra-scaled devices expected at the end-of-the-roadmap. The starting point of the model was the development of an analytical expression for the 2D distribution of the potential considering the quantum inversion charge. An extensive comparison with 2D Poisson–Schrödinger simulation data was conducted in order to fully validate the model. We have shown that the proposed model reproduces with an excellent accuracy the impact on the drain current of short-channel effects, volume inversion phenomenon and carrier quantum confinement. A very good agreement was also obtained with experimental data measured on very integrated devices. Finally, the model was implemented in Eldo IC analog simulator and the transient simulation of simple DG CMOS-based circuits has been performed.

Acknowledgements

This work was supported by the Network of Excellence SINANO and by the French National Research Agency (ANR) under the PNANO-MODERN project.

References

[1] D. Hisamoto, Short course, *Proc. IEDM Tech. Dig.*, 1 (2003).
[2] D.J. Frank, *et al.* Monte Carlo simulation of a 30 nm dual-gate MOSFET: How short can Si go? *Proc. IEDM Tech. Dig.*, 553 (1992).
[3] Y. Taur. Analytic solutions of charge and capacitance in symmetric and asymmetric Double-Gate MOSFETs. *IEEE Trans. Electron Dev.*, **48**(12), 2861 (2001).
[4] M. Chan, *et al.* Quasi-2D compact modeling for Double-Gate MOSFET. *Proc. MSM*, 108 (2004).
[5] M. Bescond, *et al.* Atomic-scale modeling of source-to-drain tunneling in ultimate Schottky barrier Double-Gate MOSFET's. *Proc. ESSDERC*, 395 (2003).
[6] M. Bescond, *et al.* Atomic-scale modeling of Double-Gate MOSFETs using a tight-binding Green's function formalism. *Solid-State Electron.*, **48**, 567 (2004).
[7] Y. Taur, *et al.* Continuous, analytic drain-current model for DG MOSFETs. *IEEE Electron Dev. Lett.*, **25**(2), 107 (2004).
[8] D. Jiménez, *et al.* Continuous analytic I–V model for surrounding-gate MOSFETs. *IEEE Electron Dev. Lett.*, **25**(8), 571 (2004).
[9] A. Ortiz-Conde, *et al.* Rigorous analytic solution for the drain current of undoped symmetric Dual-Gate MOSFETs. *Solid-State Electron.*, **49**, 640 (2005).
[10] X. Liang, Y. Taur. A 2D analytical solution for SCEs in DG MOSFETs. *IEEE Trans. Electron Dev.*, **51**(8), 1385 (2004).
[11] G. Baccarani, S. Reggiani. A compact Double-Gate MOSFET model comprising quantum-mechanical and nonstatic effects. *IEEE Trans. Electron Dev.*, **46**(8), 1656 (1999).
[12] D. Munteanu, J.L. Autran. Two-dimensional modeling of quantum ballistic transport in ultimate Double-Gate SOI devices. *Solid-State Electron.*, **47**, 1219 (2003).
[13] S. Harrison, *et al.* Electrical characterization and modeling of high-performance SON DG MOSFETs. *Proc. ESSDERC*, 373 (2004).
[14] R. Cerutti, *et al.* Design adapted planar double gate process for performant low standby power application. *Proc. Silicon Nano-workshop*, (2005).
[15] S-H. Oh, *et al.* Analytic description of short-channel effects in fully-depleted Double-Gate and cylindrical, surrounding-Gate MOSFETs. *IEEE Electron Dev. Lett.*, **21**(9), 445 (2000).
[16] A. Ortiz-Conde, *et al.* Analytic solution of the channel potential in undoped symmetric Dual-Gate MOSFETs. *IEEE Trans. Electron Dev.*, **52**(7), 1669 (2005).
[17] R.J. Van Overstraeten, *et al.* Theory of the MOS transistor in weak inversion—new method to determine the number of surface states. *IEEE Trans. Electron Dev.*, **22**(5), 282 (1975).
[18] X. Loussier, *et al.* Compact model of drain-current in Double-Gate MOSFETs including carrier quantization and short-channel effects. *Proc. NSTI-WCM*, 808 (2006).
[19] M. Alessandrini, *et al.* Development of an analytical mobility model for the simulation of ultra-thin single- and double-gate SOI MOSFETs. *Solid-State Electron.*, **48**, 589 (2004).
[20] J.A. Robinson, *et al.* A general four-terminal charging-current model for the insulated-gate field-effect transistor—I. *Solid-State Electron.*, **23**, 405 (1980).
[21] C. Turchetti, *et al.* On the small-signal behaviour of the MOS transistor in quasistatic operation. *Solid-State Electron.*, **26**, 941 (1983).
[22] Y.P. Tsividis. *Operation and modeling of the MOS transistor*, 2nd ed. McGraw-Hill, Boston (1999).